Journal of Marine Science and Engineering

MDPI

Article

Burst Pressure Prediction of API 5L X-Grade Dented Pipelines using Deep Neural Network

Dohan Oh [1], Julia Race [1], Selda Oterkus [1], Bonguk Koo [2,*]

[1] Department of Naval Architecture, Ocean and Marine Engineering, University of Strathclyde, Glasgow G4 0LZ, UK; 76odohan@gmail.com (D.O.); julia.race@strath.ac.uk (J.R.); selda.oterkus@strath.ac.uk (S.O.)

[2] Department of Naval Architecture and Marine Engineering, Changwon National University, Changwon-si, Gyeongsangnam-do 51140, Korea

* Correspondence: bonguk9@changwon.ac.kr; Tel.: +82-(055)-213-3685

Received: 29 August 2020; Accepted: 28 September 2020; Published: 30 September 2020

Abstract: Mechanical damage is recognized as a problem that reduces the performance of oil and gas pipelines and has been the subject of continuous research. The artificial neural network in the spotlight recently is expected to be another solution to solve the problems relating to the pipelines. The deep neural network, which is on the basis of artificial neural network algorithm and is a method amongst various machine learning methods, is applied in this study. The applicability of machine learning techniques such as deep neural network for the prediction of burst pressure has been investigated for dented API 5L X-grade pipelines. To this end, supervised learning is employed, and the deep neural network model has four layers with three hidden layers, and the neural network uses the fully connected layer. The burst pressure computed by deep neural network model has been compared with the results of finite element analysis based parametric study, and the burst pressure calculated by the experimental results. According to the comparison results, it showed good agreement. Therefore, it is concluded that deep neural networks can be another solution for predicting the burst pressure of API 5L X-grade dented pipelines.

Keywords: artificial neural network; deep neural network; burst pressure; pipeline; dent; ocean and shore technology (OST)

1. Introduction

Rapid industrialization and population growth have made the oil and gas industry one of the most closely associated industries with modern life and the survival of humankind, and the need to reliably supply the oil and gas to even more remote areas has emerged. Accordingly, some means to transport the oil and gas products, such as rail, truck and pipelines, have been developed. Amongst them, pipeline is known as the most efficient, cost-effective and safest method [1]. In this perspective, the accurate prediction of the burst pressure of pipelines at the design stage is critical for the safe operation [2].

In the meantime, artificial intelligence (AI) has a role as a key technology of the industry 4.0 and this state-of-the-art technology is used as a very popular and useful method in many areas. In addition, this phenomenon leads the robust growth of interest towards artificial neural network (ANN), which is an idea inspired from neural networks in the human brain and are one of the methods in machine learning. Particularly, deep neural network (DNN) is defined as the neural networks that have two or more hidden layers [3]. Furthermore, DNN is designed on the basis of ANN algorithm and is a method amongst various machine learning methods.

Tracing the application of this method, limited research has been conducted on the burst pressure of pipelines with defects using ANN, and, to date, there are no studies on the burst pressure prediction of pipelines with a dent using ANN. Xu et al. [4] applied an ANN to predict the burst pressure of corroded API X80 subsea pipelines. They concluded that the ANN predicted the burst pressure of corroded pipelines more accurately than two of the codified corrosion assessment methodologies from ASME B31G [5] and DNV-RP-F101 [6]. Liu et al. [7] also investigated the application of ANN for the prediction of the failure pressure of API X80 pipes with corrosion defects. They also concluded that the ANN model predicted more accurate results than ASME B31G [5], DNV-RP-F101 [6] and API 579 [8]. Wong et al. [9] suggested an ANN model that can predict the fatigue damage caused by the short-term vortex-induced vibration acting on the top tensioned riser. In this study, it was concluded that the ANN model could predict the fatigue damage with high accuracy and low error. Chung et al. [10] proposed a DNN model to detect a defected mooring line in tension-leg platform (TLP). From the results of this study, it was concluded that this DNN-based detection model can be used for the health monitoring of the TLP structure. Shin et al. [11] investigated the application of DNN to predict the maximum stress of a pipeline, which took actions such as pressure, wind and temperature into account. According to the results, the maximum stress of pipeline showed good agreement with the stress calculated by the numerical method.

As a result of the literature review, to date, there have been no studies on the structural integrity assessment of recessed pipelines using DNN. Therefore, it is worth developing a DNN model to predict the burst pressure of the dented pipeline. In addition, using the developed DNN model, oil and gas pipeline operators and field engineers can predict the burst pressure of API 5L X grade pipelines with an unconstrained, hemispherical, plain dent using parameters readily available in the field without conducting finite element analysis (FEA).

2. FEA Based Parametric Study

Datasets for the development of DNN model were obtained by carrying out the non-linear FEA for API 5L X52, X65 and X80 grade pipelines with a dent. The sort of dent considered in the parametric studies is an unconstrained, hemispherical, plain dent with no pipeline thickness reduction in the dent region. As the dent is unconstrained, the dent can recover elastically or rebound, after indenter removal. The FEA based parametric study (I) and (II) results were used for "training and validation" and "test". In addition, the subscripts PS(I) and PS(II) indicated hereafter denote parametric study (I) and (II), respectively.

2.1. Material Properties and Geometric Information

The used pipeline material properties for the FEA based parametric studies are listed in Table 1. The pipeline information in API 1156 [12] was used for the convenience of the validation of the FEA and DNN model, and the experimental results in API 1156 [12] were used for the test dataset. For the material properties not mentioned in API 1156 [12], the minimum values of API 5L: Specification for line pipe [13] were used.

Table 1. Material properties and geometric information for finite element analysis (FEA) based parametric study (I) [12] and (II) [13].

Heading	X52_PS(I)	X52_PS(II)	X65_PS(II)	X80_PS(II)	Outer Diameter (mm)	Thickness (mm)
Poisson's ratio	0.3				323.85	4.7752
Young's modulus (MPa)	207,000					
Yield strength (σ_{yield}, MPa)	371.60	358.53	448.16	551.58		

Ultimate tensile strength (σ_{UTS}, MPa)	529.50	455.05	530.90	620.53

2.2. Material Model

The elastic-perfectly plastic material model was used in the FEA. In the material model, tangent modulus, which represents the plastic region, has been estimated from the formula proposed by Oh et al. [2].

2.3. Definition of Finite Element Type

In order to improve the accuracy of FEA, more accurate analysis results can be obtained when the discrete error of the FEA model geometry is minimized. For this purpose, SOLID186, a high-order 3D 20 node solid element, was applied. In addition, contact elements, Targe 170 and Conta 174, were applied to the areas between the outer surface of an indenter that was an object to form a dent and pipeline outer surface. To this end, surface-to-surface contact, bonded contact behavior, augmented Lagrange formulation was recommended for general frictionless or frictional contact in large deformation problems are employed.

2.4. Applied Loading and Boundary Condition

For the FEA based parametric studies, the loading condition consisted of three steps: indentation without internal pressure (Step 1), removal of the indenter (Step 2) and application of internal pressure (Step 3) is shown in Figure 1.

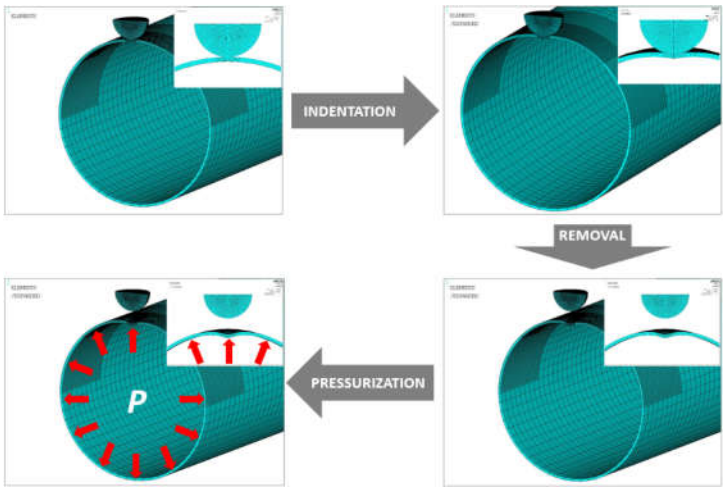

Figure 1. Loading condition of FEA.

The definition of each step is as follows;

Step 1: The pipeline is indented to the depth specified as a ratio of the pipeline outer diameter to a dent depth.

Step 2: The dented location is rebounding due to the characteristic of material, elasticity, after the removal of the indenter.

Step 3: The burst pressure of the pipeline is calculated under the condition that the internal pressure acts on the inner surface of the pipeline.

The boundary conditions were defined based on the loading condition and described in Table 2 and Figure 2. A ¼-symmetry model was employed to reduce the computational time. Therefore, Y-Z plane symmetry (Ux = 0) and X-Y plane symmetry (Uz = 0) at center of model was applied. In addition, due to the effect of the backfill at step 1 and 2, there is no displacement at the end of the pipeline (Ux = Uy = Uz = 0). In addition, it was expected that there was no displacement at the bottom

of the pipeline due to the resistance of the soil (Uy = 0). In step 3, it was assumed that the end of the pipeline could be expanded into the outward (Uz = 0) due to the globally applied internal pressure.

Table 2. Boundary condition according to the loading condition.

Loading condition	End	Top, Center	Bottom
Step 1	All fixed (Ux = Uy = Uz = 0)	Symmetry (Ux = 0, Uz = 0)	UY fixed + Symmetry (Ux = Uy = 0)
Step 2	All fixed (Ux = Uy = Uz = 0)	Symmetry (Ux = 0, Uz = 0)	UY fixed + Symmetry (Ux = Uy = 0)
Step 3	Symmetry (Uz = 0)	Symmetry (Ux = 0, Uz = 0)	UY fixed + Symmetry (Ux = Uy = 0)

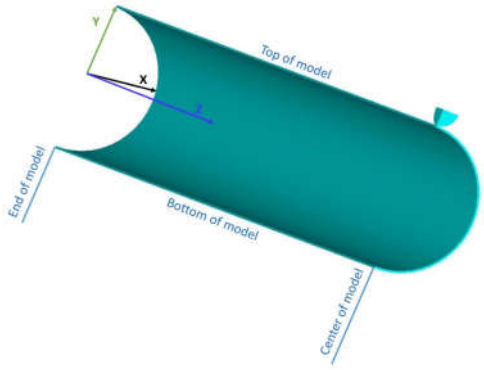

Figure 2. FEA model to describe boundary conditions.

2.5. Mesh Size and Model Length

To define the optimum mesh size and model length for the nonlinear FEA for pipelines with a dent, convergence studies were conducted and verified by comparison with FEA result and test result in API 1156 [12]. A hemispherical indenter with a diameter of 219.075 *mm* was used to construct an initial dent depth of 12% of the pipeline outer diameter. The number of elements and model length under consideration were from one to eight in the thickness direction of the FEA model and from 1.0 to 5.5 times of the pipeline diameter, respectively.

As with the results of convergence studies for the mesh size, the dent depth after removal of the indenter was almost the same regardless of the number of elements through the wall thickness between four and eight, so four was selected as the number of elements, as shown in Figure 3 below. In addition, 5.5 times of the pipeline outer diameter was selected as the model length for FEA.

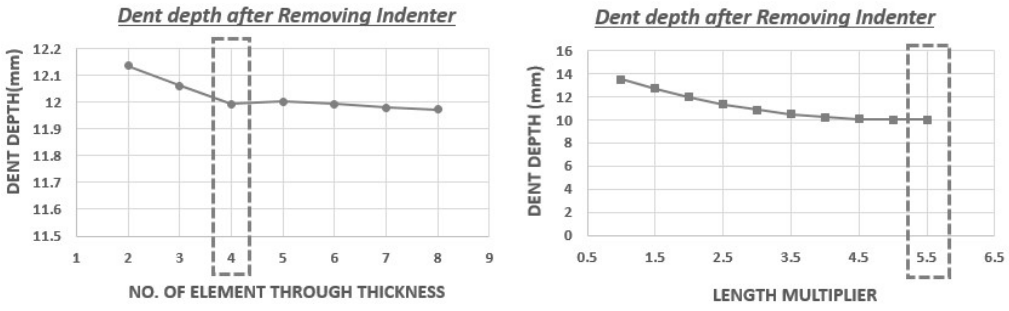

(**a**) (**b**)

Figure 3. Convergence study results: **(a)** the mesh size, **(b)** model length.

Using the mesh size and FE model length defined above, the dent shape results from this study (Applied FEA) were compared with FEA results (API 1156 FEA) and test results (API 1156 TEST) from API 1156 [12]. From comparison of results, the maximum dent depth after indenter removal was 19.05 *mm* for API 1156 FEA and API 1156 TEST and 20.75 *mm* for Applied FEA. The dent depth from API 1156 FEA and TEST was 91.8% of the Applied FEA. From this result, it can be confirmed that the Applied FEA showed conservative results. In addition, it can be said that the selected loading and boundary conditions are appropriate for this research.

2.6. Variables for FEA Based Parametric Study

For the parametric studies, initial dent depth (D_b), initial dent length (L_b) and pipeline outer diameter (D) are considered for the variables of FEA based parametric study, and the bounding cases of variables are defined in Table 3.

Table 3. Variables for the FEA based parametric study.

Design Variables	Bounding Cases		
Material	X52$_{PS(I)}$	X52$_{PS(II)}$	X65$_{PS(II)}$ and X80$_{PS(II)}$
D_b/D (%)	1-20	2.5, 5, 10, 15 and 20	
D_b/L_b (%)	2.5, 5, 7.5, 10, 12.5, 25, 37.5, 50, 75 and 100	2.5, 5, 7.5, 10, 12.5 and 25	5, 7.5, 10, 12.5 and 25

Where D_b and L_b are the initial indentation values of the dent before the rebound and these values are used for creating the dent shape on the pipelines.

2.7. Implementation

In this research, the commercial software ANSYS Mechanical APDL versions 17.1 was employed to carry out the pre-processing, solving and post-processing of nonlinear FEA for the pipelines with a dent.

3. DNN Model

The aim of this study was to develop a method that can predict the burst pressure of pipelines with a dent, and the aim of this study can be achieved and validated by conducting the investigation of the applicability of DNN to predict the burst pressure of dented pipelines.

As mentioned above, ANN is in the spotlight in all fields including engineering, and it is expected to be another solution to solve the problems relating to the pipelines. In particular, the application of DNN to the pipeline industry as a new solution to evaluate the structural integrity of pipelines with a dent seems to be a worthwhile subject to review.

In this research, a DNN model has been developed and validated to predict the burst pressure of pipelines with a dent using dataset including the FEA based parametric study results and the experimental results. The FEA based parametric study results and the experimental results for the pipelines with a hemispherical dent are listed in from Table A1 to A4 and Table A5 in the Appendix, respectively. The datasets from Table A1 to A5 are used for "training and validation" and "test".

3.1. Development of DNN

An ANN architecture, as shown in Figure 4, is composed of an input layer, hidden layers and output layer. In particular, when there are two or more hidden layers, the neural network is termed a DNN. In here, the input layer is where the data comes in and the output layer is where the model infers. The hidden layer is located between input and output layers, because the output of one layer is to be the input of the next layer. In the hidden layer, a net input is calculated, and the net input produces the actual output through an activation function, then the output transfers to the next layer. In addition, the neural network has a form connected to each neuron by the weighted link, and the

multi-layer perceptron that has multi-hidden layers between input layer and output layer is used widely.

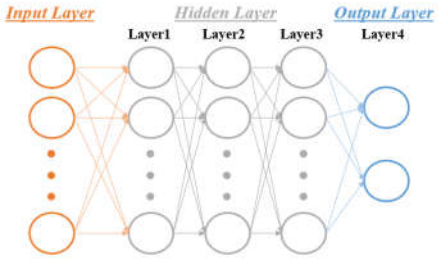

Figure 4. Diagram of the artificial neural networks.

In particular, the purpose of the use of activation functions is to calculate the weight (w) and bias (b) to minimize the errors in the output and decides the activation of the neuron based on the calculated weight and bias. The use of activation function ($f(Z)$) can impart nonlinearity to the output of neurons (P_o), and the relationship between the output of the neuron and the activation function is given in Equation (1).

$$P_O = f(Z(x)) = f\left(\sum_{i=1}^{N} w_i x_i + b\right) \quad (1)$$

where $Z(x) = \sum_{i=1}^{N} w_i x_i + b$, x_i is input and N is the number of neurons in layer.

3.2. DNN Architecture

Machine learning can be divided into supervised learning, unsupervised learning and reinforcement learning. In this study, supervised learning was applied. In particular, it focused on the DNN amongst supervised learning algorithms, and the neural network used the batch gradient descent algorithm and fully connected layer.

3.2.1. Activation Function

One of the most important factors in a neural network to obtain the best results is the selection of a suitable activation function. An activation function is used to determine whether the sum of the input causes activation or not. According to the researchers [14,15], there are many activation functions and amongst them, rectified linear unit (ReLU) is one of the best activation functions to carry out the DNN. Especially, Pedamonti [14] mentioned that ReLU is a better neuron replacing sigmoid function, and Cent et al. [15] concluded that ReLU is the best activation function after reviewing 10 activation functions. Therefore, the widely used ReLU activation function in recent years is adopted as an activation function due to the benefits of this function like faster computation and avoiding the vanishing gradient problem [14–16]. The ReLU activation function is expressed as an Equation (2) and plotted as shown in Figure 5.

$$ReLU(x) = \begin{cases} max\ (0, x), & x \geq 0 \\ 0, & x < 0 \end{cases} \quad (2)$$

where, x is the input to the neuron.

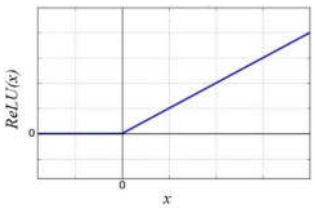

Figure 5. Rectified linear unit (ReLU) activation function.

3.2.2. Optimization

Furthermore, the broadly adopted and known as an alternative solution of the classical stochastic gradient descent method, Adam optimization algorithm [17] was selected for the optimization of the weight and bias.

3.2.3. Weight Initialization

In addition, for the initiation of the weight, He initialization [18] was chosen, and this initialization method is widely known to be specialized for the ReLU function, and is the most popular method recently.

3.2.4. Cost Function

The cost function is used to measure the error of learning, that is, how well the neural network has learned the training dataset. In this study, the mean absolute percentage error (MAPE) that is commonly used to evaluate the accuracy of forecasting [19,20] is employed as the cost function. The MAPE Equation (3) is given by as follows:

$$MAPE = \frac{100\%}{n^*}\sum_{i=1}^{n^*}\left|\frac{y_i - x_i}{y_i}\right| \quad (3)$$

where x_i is the burst pressure calculated by learning, y_i is the burst pressure from the learning data and n^* is the number of observations.

The MAPE results are interpreted based on the evaluation method proposed by Lewis [21], and is explained in Table 4.

Table 4. The guidance for the interpreting of mean absolute percentage error (MAPE) results by Lewis [21].

MAPE	Interpretation
Less than 10%	Highly accurate
Between 10% and 20%	Good
Between 20% and 50%	Reasonable
Greater than 50%	Inaccurate

In addition, Lewis [21] guideline was employed to interpret MAPE results in engineering studies [22,23]. Therefore, the Lewis [21] guideline was applied to qualitatively evaluate the MAPE results for the burst pressure prediction of pipelines with a dent.

3.2.5. Feature Normalization

The scale of all features is necessary to be transformed into the same scale, and normalization is the method to make all features to be the same scale. In this study, MinMaxScaler has been adopted to normalize the features and this scaler would transform the features into the values between 0 and 1 using Equation (4).

$$x_{norm} = \frac{x - x_{min}}{x_{max} - x_{min}} \quad (4)$$

where x is a raw data (before normalization) from a feature and x_{norm}, x_{min} and x_{max} are the normalized data, maximum and minimum value of the feature, respectively.

3.3. Application to Burst Pressure Prediction for Dented Pipelines

The FEA based parametric study results in from Table A1 to A4 and the experimental results in Table A5 in the Appendix were used to build DNN models to predict the burst pressure for dented pipelines. In addition, the considered parameters to develop the DNN model is described as follows:

3.3.1. Input and Output Parameters

(a) for input — outer diameter (D), thickness (t), dent depth (d), the ratio of dent depth to diameter, dent length after removal of indenter (L_a), the ratio of dent length after removal of indenter to diameter and ultimate tensile strength (UTS).

(b) output — the ratio of the burst pressure (P_{burst}) to UTS of the pipeline material.

3.3.2. Selection of Hyper-Parameters

Next, it needed to define hyper-parameters for the DNN model. In this study, the number of hidden layers and neurons, size of epoch and learning rate were taken into account and the values were defined through the trade-off studies as listed in Table 5.

Table 5. Subject to trade-off studies for defining hyperparameters for pipelines with a dent.

Hyper-Parameters	Sample
Number of hidden layers	2, 3, and 4
Number of neurons	8×4×2, 27×9×3, 64×16×4 and 125×25×5
Epoch size	10, 100, 1000, 2000, 3000 and 4000
Learning rate (10^{-3})	50, 10, 5, 1, 0.9, 0.8, 0.7, 0.6, 0.5 and 0.1

Number of Hidden Layers

The number of hidden layers of the DNN model were examined for two, three and four. In the results of trade-off study shown in Figure 6, the MAPE according to the number of hidden layers, two, three and four, are 0.12%, 0.027% and 0.048%, respectively. According to Table 4, the MAPEs for all cases indicate high accuracy, therefore, whichever one amongst the three cases is selected, it is expected not to effect on the output. Finally, three hidden layers with the lowest MAPE were observed and employed in the DNN model.

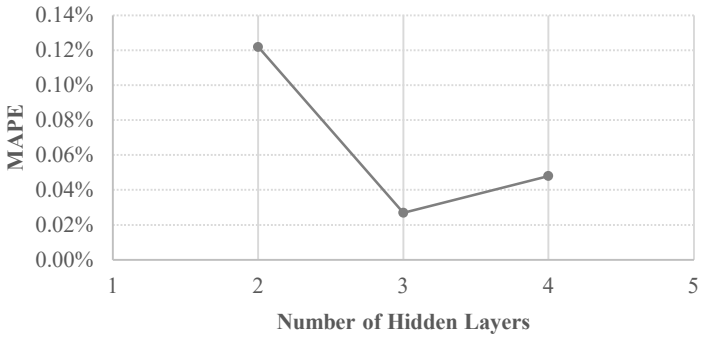

Figure 6. Selection of the number of hidden layers for the deep neural network (DNN) model.

Number of Neurons

According to Panchal et al. [24], the number of neurons in hidden layers might have an effect on the overfitting or underfitting problem. There are some ways to handle the overfitting problem, like controlling the number of layers or neurons, regularization and dropout. In this research, to determine the number of neurons in the hidden layer of the DNN model, a trade-off study was performed considering the cases of 8×4×2, 27×9×3, 64×16×4 and 125×25×5, and the results are shown in Figure 7a,b. From the result depicted in Figure 7a, the overfitting or underfitting problem was not found in all cases and the results of MAPEs seen in Figure 7b are 1.39%, 0.34%, 0.33% and 0.35%, respectively. Finally, 64×16×4, the lowest MAPE result, was selected as the number of neurons in the hidden layer.

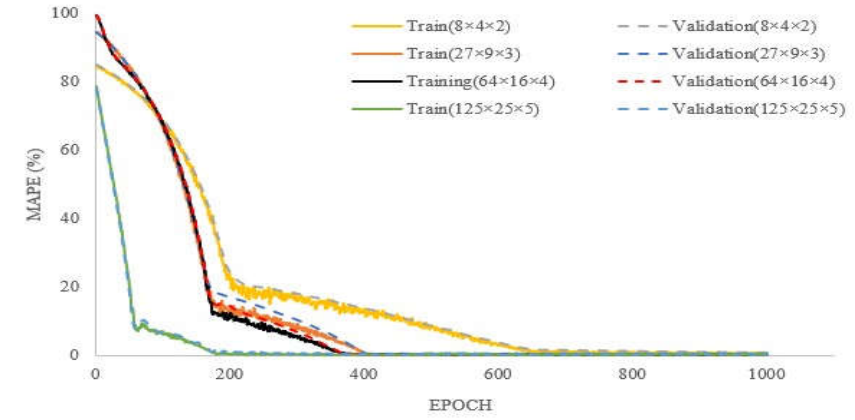

(**a**)

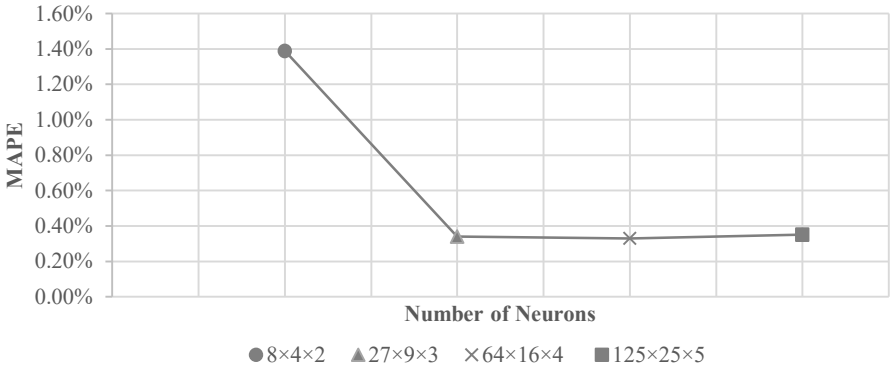

(**b**)

Figure 7. Selection of the number of neurons for the DNN model: (**a**) **a**ccuracy of DNN model with training and validation in terms of MAPE. (**b**) **a**ccuracy of DNN model with test in terms of MAPE. .

Size of Epoch

Epoch is defined as the status that the learning has completed through the forward propagation and backward propagation over the entire training dataset, and the selection of the proper size of epochs is critical against preventing the under-fitting or over-fitting problems. Therefore, for the DNN model epoch sized of 10, 100, 1000, 2000, 3000 and 4000 were considered. The findings of the trade-off studies are shown in Figure 8, the MAPE was observed to converge 0% from epoch size 1000. The lowest MAPE (=0.03%) was observed at epoch size 1000, 3000 and 4000. According to Table 4, MAPEs for all cases indicate high accuracy, and finally epoch size 1000 was employed for the DNN model.

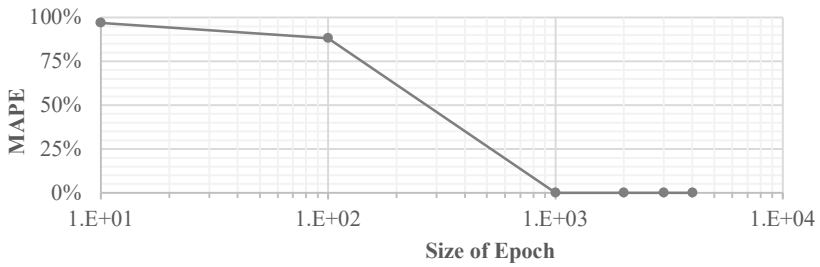

Figure 8. Selection of the epoch size for the DNN model.

Learning Rate

The learning rate is related to the determination of the update of weight. If the learning rate is too small, it may lead to long learning times. On the other hand, a too high learning rate may result in non-convergence. Therefore, the learning rate needs to be appropriately adjusted according to the DNN model. In total, ten different learning rates as illustrated in Table 5 were considered to determine the learning rate. The resultant MAPE, according to the learning rate, is presented in Figure 9, and this can be interpreted as highly accurate based on Table 4. According to the results, the selected learning rate with the lowest MAPE (=0.08%) is 0.001.

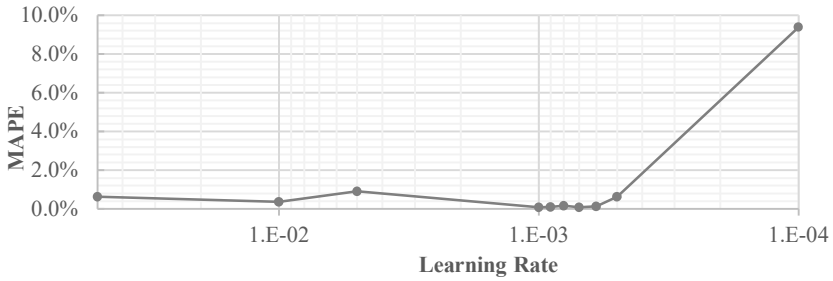

Figure 9. Selection of the learning rate for the DNN model.

The summary of the hyper-parameters for DNN model is described in Table 6 and the defined DNN diagram is depicted in Figure 10.

Table 6. Summary of the defined hyper-parameters for deep neural network model.

	Number of Hidden Layer	Size of epoch	Learning rate
Pipelines with a dent	3	1000	0.001

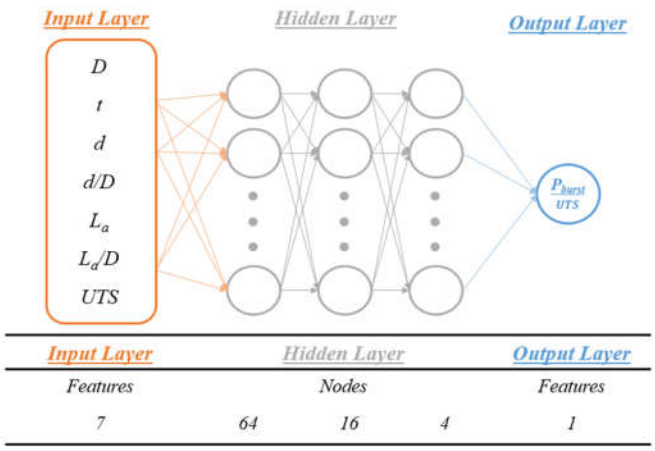

Figure 10. Defined DNN diagram

3.4. Implementation

Selection of the programming language for the best use of AI is important, and especially for the DNN implementation. In this research, Python was used as a programming language to develop the DNN model to predict the burst pressure of pipelines with or without a dent. In addition, TensorFlow, which provides an open-source library for neural networks, was adopted as the framework. For the last, Jupyter notebook, which is an integrated development and learning environment in Python, was selected as an interface.

4. Results

In the case of pipelines with a hemispherical dent, the DNN model has been developed based on the 150 data from the FEA based parametric study (I) results as listed in Table A1 in the Appendix. In addition, the FEA based parametric study (II) and experimental test results as listed in Table A2 to A5 in the Appendix were used to validate the applicability of the developed DNN model to predict the burst pressure. The proportion of "training and validation dataset" and "test dataset" in the total data is 83% and 17%, respectively. In here, "training and validation dataset" is randomly split at a ratio of 80% to 20%.

As shown in Figure 11, the accuracy of DNN model for the pipelines with a hemispherical dent with training and validation in terms of MAPE is visualized across the epoch.

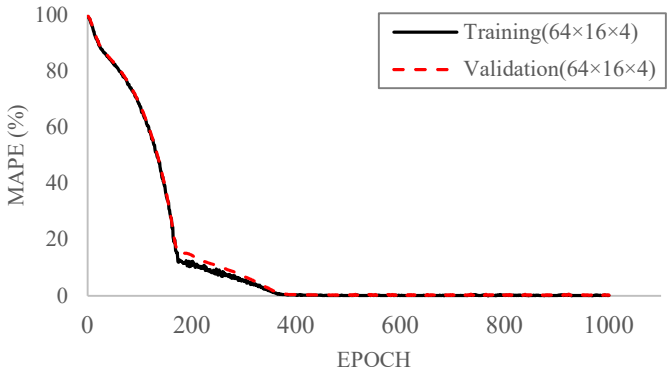

Figure 11. Accuracy of DNN model with training and validation in terms of MAPE.

In fact, the MAPE of training shows the convergency at about 400 epochs, however, the DNN model has kept the training up to 1,000 epochs to investigate the overfitting. If the difference between the validation MAPE and the training MAPE is getting bigger and bigger even though the training MAPE is converging to the minimum, this means overfitting occurred [10]. According to the accuracy of DNN model, the MAPEs of training and validation are congregated 0.08% and 0.17%, respectively, and it shows the converging and stabilizing of the DNN model. In addition, the resultant MAPEs from the training and validation stages can be interpreted as highly accurate based on Table 4.

4.1. Comparison with FEA Based Parametric Study Results

For the validation of the DNN model for the pipeline with a hemispherical dent, the burst pressure computed by the DNN model has been compared with the burst pressure determined by the FEA. The comparison of results has been performed by correlation analysis to examine the relationship as well as by statistical analysis to determine the accuracy of prediction, and Pearson's product-moment correlation coefficient (PPMCC) and MAPE were used, respectively. The PPMCC is commonly used as a measure of the linear relationship between two quantitative variables and is calculated by the following Equation (5):

$$PPMCC\ (r) = \frac{\sum(x-\bar{x})(y-\bar{y})}{\sqrt{\sum(x-\bar{x})^2\sum(y-\bar{y})^2}} \quad (5)$$

where x and y are the burst pressure calculated by the FEA or experiments and by the DNN model, respectively, and $\bar{x}$ and $\bar{y}$ are the average values of x and y groups of values, respectively.

As indicated by the correlation analysis result as shown in Figure 12, the PPMCC depending on the pipeline material is distributed between 0.959 and 1.0.

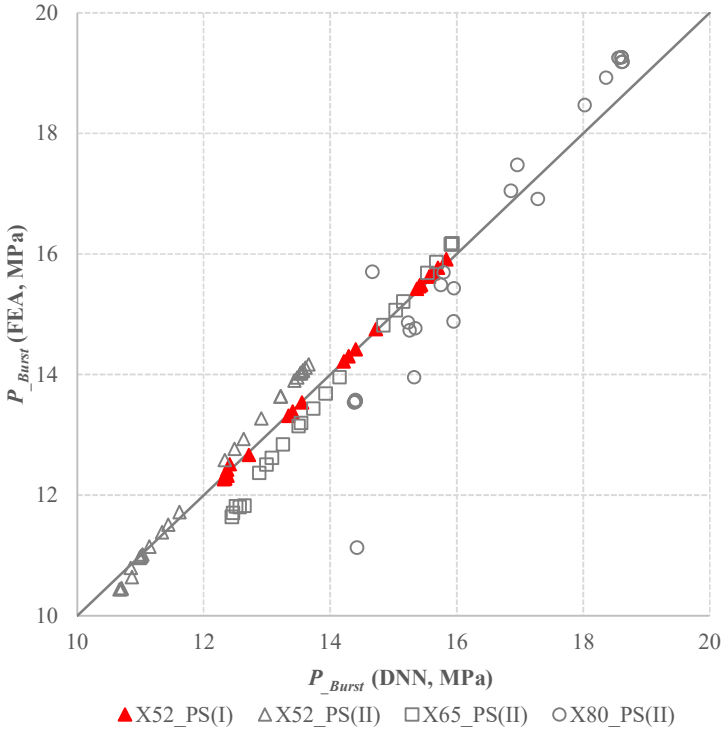

Figure 12. Pearson's product-moment correlation coefficient (PPMCC) between the burst pressure computed by the DNN model and the FEA based parametric study results for the pipeline with a hemispherical dent.

Based on the Evans guidance listed in Table 7, these values indicate a very strong positive relationship between the burst pressure calculated by the DNN model and by the FEA. Evans [25] proposed guidance for the strength of the correlation expressed by the limit of the absolute *r*-value (PPMCC) as shown in Table 7.

Table 7. The guidance for the strength of the correlation by Evans [25].

PPMCC (*r*)	Strength
0.00–0.19	very weak
0.20–0.39	weak
0.40–0.59	moderate
0.60–0.79	strong
0.80–1.00	very strong

The prediction accuracy (measured using MAPE) of the burst pressure from the DNN model and FEA for the $X52_{PS(I)}$, $X52_{PS(II)}$, $X65_{PS(II)}$ and $X80_{PS(II)}$ dataset is 0.33%, 2.17%, 2.81% and 5.55%, respectively. The obtained MAPEs can be interpreted as highly accurate based on Table 4. According to the results, it can be said that DNN is able to reliably estimate the burst pressure of the pipeline with a hemispherical dent.

4.2. Comparison with Experimental Results

The reliability of the DNN model was validated by performing correlation and statistical analysis between the burst pressure calculated by the DNN model and the three results of the experiment from the published papers [12,26]. The detailed information is as listed in Table A5 in the Appendix. In accordance with the correlation analysis results between the DNN model and experiments as shown in Figure 13, the PPMCC is 1.000 and the MAPE is 1.52%. The PPMCC

interpreted by the Evans guidance listed in Table 7 and MAPE interpreted by the Lewis guidance listed in Table 4 indicates a very strong positive, highly accurate relationship between the burst pressure computed by the DNN model and the experimental test results.

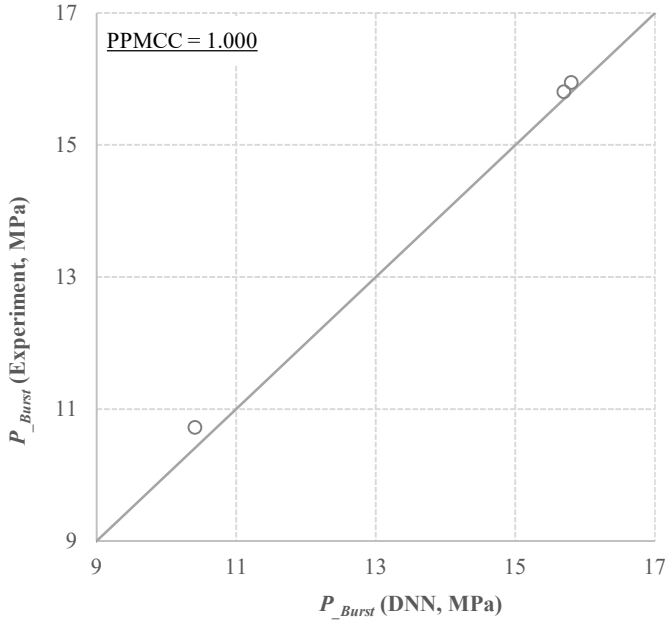

Figure 13. PPMCC between the burst pressure computed by the DNN model and the experimental results for the pipeline with a hemispherical dent.

From the above results in Section 4.1 to 4.2, the predicted burst pressure by the DNN model corresponded well with the results of the FEA and the experimental test.

5. Discussion

The aim of this research is to develop a method to predict the burst pressure of API 5L X grade pipelines with an unconstrained, hemispherical, plain dent using parameters readily available in the field without conducting FEA.

To date, the structural integrity of pipelines with a dent has been used for the allowance of the dent depth according to the codes and regulations like ASME B31.8 [27], the American Petroleum Institute API 1156 [12], the European Pipeline Research Group (EPRG) [28] and the Pipeline Defect Assessment Manual (PDAM) [29] applies predominantly 6% or 7% of pipeline diameter. However, the mentioned above defect assessment methodologies currently in use focuses on the dent depth and are recognized as conservative methods. This means that these methodologies are not reasonable from an economic perspective.

Woo et al. [30] conducted a study to examine the structural integrity of a dented pipeline using ANN. They have estimated the maximum equivalent plastic strain and the maximum difference in the stress component in the pipe (in the respective direction; hoop and axial). In addition, they have conducted the prediction of the longitudinal and circumferential radii. Especially, the maximum equivalent plastic strain estimated by ANN has been compared with the strain calculated by ASME B31.8 [27]. According to the comparison result, the maximum equivalent plastic strain estimated by ANN has a good agreement with the FEA analysis results than the strain calculated by ASME B31.8 [27].

However, above mentioned codes, regulations and the ANN model cannot estimate the burst pressure of pipelines with a dent.

Therefore, to achieve the aim, DNN model has been developed to estimate the burst pressure for API 5L X grade pipelines with an unconstrained, plain dent. The developed DNN models used

the FEA based Parametric Study results and validated by comparison with the FEA based Parametric Study results and the experimental results. The reliability of the DNN models has been investigated by performing the correlation and statistical analysis between the burst pressure computed by the DNN model and the FEA based parametric study results and by the experimental results.

According to the validation results, it can be seen that the MAPE value for each test increases slightly as the yield and ultimate tensile strength of the pipeline material increase. The reason is that because the developed DNN model was trained using X52 pipeline dataset, it could not learn the effect of the different material properties, and it can be inferred that this affected the results.

Nevertheless, the results of burst pressure computed by the DNN model corresponded well with the nonlinear FEA based parametric study results and the burst pressure results of the experiment.

Consequently, using the DNN model, operators and field engineers can not only calculate the capacity of the dented pipelines without carrying out the expensive FEA on every dent but also can make efficient repair decisions.

6. Conclusion

From the research findings the following conclusions can be drawn:

1) The applicability of the DNN as a new solution to predict the burst pressure of pipelines with a dent has been studied.
2) The FEA based parametric study results and the experimental results for the pipelines with a hemispherical dent, and the pipelines with a spheroidal dent have been used to develop the DNN model.
3) The reliability of the DNN model was investigated by performing the correlation (PPMCC) and statistical (MAPE) analysis of the burst pressure computed using the DNN model and using the nonlinear FEA and the experimental test results.
4) According to the PPMCC and MAPE as summarized in Table 8, all figures indicate that the results of burst pressure computed by the DNN model corresponded well with the nonlinear FEA based parametric study results and the burst pressure results of the experiment.

Table 8. Summary of PPMCCs and MAPEs based on the burst pressure predicted by FEA and DNN.

Dent Shape	(A)	(B)	Between (A) and (B)		Remarks
			PPMCC	MAPE (%)	
Hemi-Spherical	**FEA**	**DNN**	1.000	0.33	$X52_{PS(I)}$
	FEA	DNN	0.999	2.17	$X52_{PS(II)}$
	FEA	DNN	0.999	2.81	$X65_{PS(II)}$
	FEA	DNN	0.959	5.55	$X80_{PS(II)}$
	Experiment	DNN	1.000	1.52	X52 (1)~(3)

Author Contributions: Conceptualization, D.O., J.R. and S.O.; methodology, D.O., J.R. and S.O.; software, D.O. and B.K.; validation, D.O.; formal analysis, D.O.; investigation, D.O.; resources, D.O. and J.R.; data curation, D.O. and B.K.; writing—original draft preparation, D.O., J.R. and B.K.; writing—review and editing, D.O., J.R., S.O. and B.K.; visualization, D.O.; supervision, J.R. and S.O. All authors have read and agreed to the published version of the manuscript.

Funding: This research received no external funding.

Conflicts of Interest: The authors declare no conflict of interest.

Appendix

Table A1. *La*, *La*/*D*, *Da*, *Da*/*D* and burst pressure for the FEA based parametric study (I).

No.	D_a/D (%)	L_a (*mm*)	L_a/D (%)	Burst pressure (MPa)	No.	D_a/D (%)	L_a (*mm*)	L_a/D (%)	Burst pressure (MPa)
1	1	152.06	46.95	15.84	51	6	180.85	55.84	15.48
2	1	83.44	25.76	15.87	52	6	114.59	35.39	15.49
3	1	58.91	18.19	15.90	53	6	94.79	29.27	15.37
4	1	48.15	14.87	15.83	54	6	85.91	26.53	14.64
5	1	42.68	13.18	15.90	55	6	80.97	25.00	14.01
6	1	32.67	10.09	15.81	56	6	73.15	22.59	12.32
7	1	28.42	8.78	14.08	57	6	71.10	21.95	12.29
8	1	25.69	7.93	14.21	58	6	70.74	21.84	12.34
9	1	22.88	7.07	14.39	59	6	70.18	21.67	12.33
10	1	21.47	6.63	14.46	60	6	69.97	21.61	12.33
11	2	158.29	48.88	15.70	61	7	186.35	57.54	15.44
12	2	88.35	27.28	15.74	62	7	121.83	37.62	15.45
13	2	64.95	20.06	15.74	63	7	102.92	31.78	15.30
14	2	54.25	16.75	15.60	64	7	94.74	29.25	14.40
15	2	48.55	14.99	15.48	65	7	90.24	27.86	13.67
16	2	38.77	11.97	14.40	66	7	83.12	25.67	12.29
17	2	35.12	10.84	13.37	67	7	81.37	25.12	12.26
18	2	33.39	10.31	13.45	68	7	80.98	25.01	12.33
19	2	31.40	9.69	13.55	69	7	80.53	24.87	12.32
20	2	30.43	9.40	13.59	70	7	80.37	24.82	12.32
21	3	164.34	50.75	15.59	71	8	194.78	60.14	15.43
22	3	93.27	28.80	15.62	72	8	130.93	40.43	15.43
23	3	70.98	21.92	15.59	73	8	112.65	34.78	15.24
24	3	60.34	18.63	15.36	74	8	104.85	32.38	14.29
25	3	54.42	16.80	15.06	75	8	100.63	31.07	13.47
26	3	44.86	13.85	12.98	76	8	93.97	29.02	12.28
27	3	41.82	12.91	12.66	77	8	92.41	28.53	12.25
28	3	41.10	12.69	12.69	78	8	92.01	28.41	12.34
29	3	39.91	12.32	12.72	79	8	91.60	28.29	12.35
30	3	39.39	12.16	12.72	80	8	91.47	28.24	12.35
31	4	169.84	52.44	15.55	81	9	203.71	62.90	15.43
32	4	100.13	30.92	15.57	82	9	141.21	43.60	15.43
33	4	78.53	24.25	15.50	83	9	123.61	38.17	15.18
34	4	68.25	21.08	15.12	84	9	116.07	35.84	14.28
35	4	62.44	19.28	14.69	85	9	112.05	34.60	13.40
36	4	53.22	16.43	12.38	86	9	105.70	32.64	12.30
37	4	50.56	15.61	12.35	87	9	104.23	32.18	12.27
38	4	50.25	15.52	12.36	88	9	103.82	32.06	12.38
39	4	49.47	15.28	12.35	89	9	103.41	31.93	12.42
40	4	49.17	15.18	12.34	90	9	103.28	31.89	12.42
41	5	175.35	54.14	15.51	91	10	212.64	65.66	15.42
42	5	107.36	33.15	15.53	92	10	151.48	46.78	15.42
43	5	86.66	26.76	15.44	93	10	134.56	41.55	15.11
44	5	77.08	23.80	14.88	94	10	127.29	39.31	14.28
45	5	71.70	22.14	14.35	95	10	123.46	38.12	13.34
46	5	63.19	19.51	12.35	96	10	117.43	36.26	12.31
47	5	60.83	18.78	12.32	97	10	116.05	35.83	12.30
48	5	60.49	18.68	12.35	98	10	115.63	35.71	12.42
49	5	59.83	18.47	12.34	99	10	115.22	35.58	12.48
50	5	59.57	18.39	12.33	100	10	115.10	35.54	12.49

Table A1. (*Cont.*) *La*, *La*/*D*, *Da*, *Da*/*D* and burst pressure for the FEA based parametric study (I).

No.	D_a/D (%)	L_a (*mm*)	L_a/D (%)	Burst pressure (MPa)	No.	D_a/D (%)	L_a (*mm*)	L_a/D (%)	Burst pressure (MPa)
101	11	221.57	68.42	15.41	126	13	154.11	47.59	12.37
102	11	161.75	49.95	15.42	127	13	152.95	47.23	12.36
103	11	145.52	44.93	15.05	128	13	152.54	47.10	12.45
104	11	138.51	42.77	14.28	129	13	152.16	46.99	12.53
105	11	134.88	41.65	13.27	130	13	152.07	46.96	12.54
106	11	129.15	39.88	12.33	131	14	262.09	80.93	15.37
107	11	127.86	39.48	12.32	132	14	197.81	61.08	15.37
108	11	127.44	39.35	12.45	133	14	182.42	56.33	14.72
109	11	127.02	39.22	12.55	134	14	175.71	54.26	14.06
110	11	126.91	39.19	12.56	135	14	172.26	53.19	13.11
111	12	234.04	72.27	15.40	136	14	166.99	51.56	12.39
112	12	172.96	53.41	15.41	137	14	165.87	51.22	12.37
113	12	157.09	48.51	14.97	138	14	165.49	51.10	12.43
114	12	150.23	46.39	14.24	139	14	165.15	51.00	12.48
115	12	146.72	45.31	13.21	140	14	165.06	50.97	12.48
116	12	141.23	43.61	12.35	141	15	276.11	85.26	15.35
117	12	140.02	43.23	12.34	142	15	210.24	64.92	15.35
118	12	139.59	43.10	12.47	143	15	195.09	60.24	14.60
119	12	139.17	42.97	12.58	144	15	188.45	58.19	13.96
120	12	139.07	42.94	12.59	145	15	185.02	57.13	13.07
121	13	248.06	76.60	15.38	146	15	179.87	55.54	12.42
122	13	185.39	57.24	15.39	147	15	178.80	55.21	12.39
123	13	169.75	52.42	14.84	148	15	178.44	55.10	12.41
124	13	162.97	50.32	14.15	149	15	178.14	55.01	12.43
125	13	159.49	49.25	13.16	150	15	178.05	54.98	12.43

Table A2. *La*, *La*/*D*, *Da*, *Da*/*D* and burst pressure for the FEA based parametric study (II) for X52 material pipelines with a hemispherical dent.

No.	L_a (*mm*)	L_a/D (%)	D_a (*mm*)	D_a/D (%)	Burst pressure (MPa)	No.	L_a (*mm*)	L_a/D (%)	D_a (*mm*)	D_a/D (%)	Burst pressure (MPa)
1	166.984	51.56	2.248	0.69	14.172	16	97.068	29.97	24.236	7.48	11.509
2	84.334	26.04	3.076	0.95	14.071	17	94.224	29.09	24.179	7.47	10.794
3	59.644	18.42	3.654	1.13	14.067	18	87.176	26.92	24.235	7.48	10.963
4	49.274	15.22	3.946	1.22	14.025	19	226.618	69.98	37.061	11.44	13.643
5	43.692	13.49	4.133	1.28	14.022	20	167.120	51.60	37.575	11.60	13.271
6	32.306	9.98	4.447	1.37	12.769	21	151.080	46.65	37.780	11.67	11.388
7	160.556	49.58	9.159	2.83	14.113	22	142.542	44.01	37.777	11.66	11.016
8	93.538	28.88	10.352	3.20	14.036	23	138.960	42.91	37.836	11.68	10.982
9	72.252	22.31	10.678	3.30	14.02	24	133.504	41.22	37.915	11.71	10.994
10	61.582	19.02	10.792	3.33	12.584	25	271.870	83.95	50.396	15.56	13.635
11	55.898	17.26	10.894	3.36	11.722	26	220.318	68.03	51.352	15.86	10.645
12	45.600	14.08	11.016	3.40	11.148	27	202.902	62.65	51.520	15.91	10.442
13	188.400	58.18	23.611	7.29	13.952	28	193.310	59.69	51.592	15.93	10.461
14	124.728	38.51	23.883	7.37	13.902	29	190.790	58.91	51.616	15.94	10.444
15	105.548	32.59	24.150	7.46	12.935	30	181.872	56.16	51.740	15.98	10.439

Table A3. *La, La/D, Da, Da/D* and burst pressure for the FEA based parametric study (II) for X65 material pipelines with a hemispherical dent.

No.	L_a (*mm*)	L_a/D (%)	D_a (*mm*)	D_a/D (%)	Burst pressure (MPa)	No.	L_a (*mm*)	L_a/D (%)	D_a (*mm*)	D_a/D (%)	Burst pressure (MPa)
1	82.094	25.35	2.497	0.77	16.177	14	90.004	27.79	22.877	7.06	13.147
2	57.694	17.82	3.014	0.93	16.175	15	82.112	25.35	22.980	7.10	13.196
3	47.812	14.76	3.321	1.03	16.164	16	162.912	50.30	35.670	11.01	13.684
4	42.462	13.11	3.525	1.09	16.159	17	147.470	45.54	35.943	11.10	12.841
5	30.982	9.57	3.835	1.18	15.688	18	139.186	42.98	35.958	11.10	12.367
6	90.044	27.80	9.220	2.85	16.175	19	135.394	41.81	36.027	11.12	12.510
7	69.532	21.47	9.723	3.00	16.161	20	127.718	39.44	36.105	11.15	12.620
8	59.322	18.32	9.924	3.06	15.866	21	215.576	66.57	49.110	15.16	11.824
9	53.734	16.59	10.070	3.11	15.214	22	198.768	61.38	49.322	15.23	11.804
10	43.190	13.34	10.267	3.17	13.954	23	189.740	58.59	49.390	15.25	11.643
11	120.920	37.34	22.533	6.96	15.067	24	184.762	57.05	49.430	15.26	11.707
12	102.568	31.67	22.708	7.01	14.819	25	182.062	56.22	49.536	15.30	11.814
13	94.104	29.06	22.814	7.04	13.435						

Table A4. *La, La/D, Da, Da/D* and burst pressure for the FEA based parametric study (II) for X80 material pipelines with a hemispherical dent.

No.	L_a (*mm*)	L_a/D (%)	D_a (*mm*)	D_a/D (%)	Burst pressure (MPa)	No.	L_a (*mm*)	L_a/D (%)	D_a (*mm*)	D_a/D (%)	Burst pressure (MPa)
1	80.120	24.74	2.024	0.62	19.251	14	86.702	26.77	21.372	6.60	15.434
2	56.824	17.55	2.463	0.76	19.251	15	78.958	24.38	21.499	6.64	15.705
3	46.910	14.49	2.738	0.85	19.186	16	158.490	48.94	33.651	10.39	15.697
4	41.728	12.88	2.936	0.91	19.184	17	142.794	44.09	33.948	10.48	14.734
5	32.042	9.89	3.305	1.02	19.261	18	135.372	41.80	34.001	10.50	14.885
6	86.732	26.78	7.901	2.44	19.261	19	131.820	40.70	34.091	10.53	14.767
7	66.800	20.63	8.605	2.66	18.925	20	126.242	38.98	34.201	10.56	14.861
8	57.222	17.67	8.902	2.75	18.472	21	209.458	64.68	46.638	14.40	13.543
9	51.904	16.03	9.100	2.81	17.048	22	193.632	59.79	46.953	14.50	13.575
10	41.518	12.82	9.373	2.89	13.954	23	189.740	58.59	49.390	15.25	13.560
11	117.008	36.13	20.949	6.47	17.479	24	184.762	57.05	49.430	15.26	13.546
12	99.282	30.66	21.153	6.53	16.914	25	182.062	56.22	49.536	15.30	11.133
13	90.790	28.03	21.280	6.57	15.489						

Table A5. Validation information from the experimental result of the hemispherical dent [12,26].

Characteristics	X52 (1)	X52 (2)	X52 (3)
Outer diameter (mm)	323.85	323.85	720
Thickness (mm)	4.7752	4.7752	8.1
Dent depth (mm)	34.773	25.654	48.68
Dent length (mm)	171.06	147.72	271.15
Yield strength (MPa)	371.6	371.6	375
Ultimate tensile strength (MPa)	529.5	529.5	468
Burst pressure, Experiment (MPa)	15.81	15.95	10.72

References

1. Green, K.P.; Jackson, T. *Safety in the Transportation of Oil and Gas: Pipelines or Rail?* Fraser Research Bulletin by the Fraser Institute: Vancouver, BC, Canada, 2015.
2. Oh, D.H.; Race, J.; Oterkus, S.; Chang, E.R. A new methodology for the prediction of burst pressure for API 5L X grade flawless pipelines. *Ocean Eng.* **2020**, *212*, 107602, doi:10.1016/j.oceaneng.2020.107602.
3. Nielsen, M.A. Using neural nets to recognize handwritten digits. In *Neural Networks and Deep Learning*; 2015. Available online: http://neuralnetworksanddeeplearning.com/ (accessed on 30 September 2020)
4. Xu, W.; Li, C.B.; Choung, J.; Lee, J. Corroded pipeline failure analysis using artificial neural network scheme. *Adv. Eng. Softw.* **2017**, *112*, 255–266.
5. ASME. Manual for determining the remaining strength of corroded pipelines. In *ASME B31G*. American Society Mechanical Engineers: New York, USA, 2012.
6. DNV. Corroded pipelines. In *Recommended Practice DNV-RP-F101*. Det Norske Veritas: Oslo, Norway, 2008.
7. Liu, X.; Xia, M.; Bolati, D.; Liu, J.; Zheng, Q.; Zhang, H. An ANN-based failure pressure prediction method for buried high-strength pipes with stray current corrosion effect. *Energy Sci. Eng.* **2020**, *8*, 248–259.
8. API. Fitness-for-service. In *API 579-1/ASME FFS-1*; American Petroleum Institute: Washington, DC, USA, 2016.
9. Wong, E.W.C.; Kim, D.K. A simplified method to predict fatigue damage of TTR subjected to short-term VIV using artificial neural network. *Adv. Eng. Softw.* **2018**, *126*, 100–109.
10. Chung, M.W.; Kim, S.J.; Lee, K.H.; Shin, D.H. Detection of damaged mooring line based on deep neural networks. *Ocean. Eng.* **2002**. *209*, 107522, doi:10.1016/j.oceaneng.2020.107522.
11. Shin, S.C.; Oh, S.J.; Lim, C.O.; Park. B.C.; Lee, J.C. Deep neural networks for maximum stress prediction in piping design, *Int. J. Fuzzy Log. Intell. Syst.* **2019**, *19*, 140–146.
12. Alexander, C.R.; Kiefner, J.F. Effects of smooth and rock dents on liquid petroleum pipelines. In Proceedings of the API Pipeline Conference, Dallas, TX, USA, 10 October 1997.
13. API. *API 5L: Specification for Line Pipe*; American Petroleum Institute: Washington, DC, USA, 2004.
14. Pedamonti, D. Comparison of non-linear activation functions for deep neural networks on MNIST classification task. *arXiv Prepr.* **2018**, arXiv:1804.02763. Available online: http://arxiv.org/abs/1804.02763 (accessed on 8 April 2018).
15. Bircanoğlu, C. A comparison of activation functions in artificial neural networks. In Proceedings of the 2018 26th Signal Processing and Communications Applications Conference (SIU), Izmir, Turkey, 2–5 May 2018.
16. Shin, S.C.; Kim, G.Y.; Ban, I.J.; Park, B.C.; Oh, S.J.; Lim, C.O. Estimation of lightweight in the initial design of ships using deep neural networks. *J. Korean Ins Intell. Syst* **2019**, *29*, 416–423.
17. Kingma, D.P.; Ba, J. Adam: A method for stochastic optimization. In Proceedings of the 3rd International Conference for Learning Representations, San Diego, CA, USA, 7–9 May 2015.
18. He, K.; Zhang, X.; Ren, S.; Sun, J. Delving Deep into Rectifiers: Surpassing Human-Level Performance on ImageNet Classification. Arxiv. Available online: https://arxiv.org/abs/1502.01852 (accessed on 6 February 2015).
19. Chen, R.J.C.; Bloomfield, P.; Fu, J.S. An evaluation of alternative forecasting methods to recreation visitation. *J. Leis. Res.* **2003**, *35*, 441–454.
20. Shen, S.; Li, G.; Song, H. Effect of seasonality treatment on the forecasting performance of tourism demand models. *Tour. Econ.* **2019**, *15*, 693–708.
21. Lewis, C.D. *Industrial and Business Forecasting Methods: A Practical Guide to Exponential Smoothing and Curve Fitting*; Butterworth Scientific: London, UK, 1982.
22. Hung, C.C.; Wang, C.C.; Wang, H.Y. Establishment of the controlled low-strength desulfurization slag prediction model for compressive strength and surface resistivity. *Appl. Sci.* **2020**, *10*, 5674, doi:10.3390/app10165674.
23. Chen, H.; Chen, W.; Zhou, Y. Estimation of chromaticity coordinates for LEDs array by modulation of red or yellow LEDs with artificial neural network. In Proceedings of the 2013 Ninth International Conference on Intelligent Information Hiding and Multimedia Signal Processing, Beijing, China, 16–18 October 2013; pp. 88–91, doi:10.1109/IIH-MSP.2013.31.
24. Panchal, F.S.; Panchal, M. Review on methods of selecting number of hidden nodes in artificial neural network. *Inter. J. Comput. Sci Mob. Comput.* **2014**, *3*, 455–464.
25. Evans, J.D. *Straightforward Statistics for the Behavioral Sciences*; Brooks/Cole Publishing Company: Pacific Grove, CA, USA, 1996.

26. Shuai, Y.; Shuai, J.; Zhang, X. Experimental and numerical investigation of the strain response of a dented API 5L X52 pipeline subjected to continuously increasing internal pressure. *J. Nat. Gas. Sci. Eng.* **2018**, *56*, 81–92.
27. ASME. Gas transmission and distribution piping systems. In *ASME B31.8*; American Society Mechanical Engineers: New York, NY, USA, 2014.
28. Roovers, P.; Bood, R.; Galli, M.; Marewski, U.; Steiner, M.; Zaréa, M. EPRG methods for assessing the tolerance and resistance of pipelines to external damage. In *Third International Pipeline Technology Conference, Brugge, Belgium, 21–24 May 2000*; Denys, R., Ed.; Elsevier Science: Amsterdam, The Netherland, 2020; Volume II, pp. 405–425.
29. Cosham, A.; Hopkins, P. The effect of dents in pipelines-guidance in the pipeline defect assessment manual. *Int. J. Press. Vessel. Pip.* **2004**, *81*, 127–139.
30. Woo, J.; Kainat, M.; Okoloekwe, C.; Hassanien, S.; Adeeb, S. Integrity analysis of dented pipelines using artificial neural networks. *Pipeline Sci. Tech.* **2019**, *3*, 92–104.